Control Methodologies for a Heterogeneous Group of Untethered Magnetic Micro-Robots

Steven Floyd*, Eric Diller, Chytra Pawashe†, and Metin Sitti‡

Abstract

In this work, we develop methods for controlling multiple untethered magnetic micro-robots (Mag-μBots) without the need for a specialized substrate. We investigate Mag-μBots that are geometrically and magnetically designed to respond uniquely to the same input magnetic fields. Designs include: (1) geometrically similar Mag-μBots with different values of magnetization, (2) geometrically dissimilar Mag-μBots with similar magnetization, and (3) geometrically dissimilar Mag-μBots with dissimilar magnetization. The responses of both magnetically hard and soft Mag-μBots are investigated. By controlling the input magnetic fields, individual and sub-groups of Mag-μBots are able to locomote in a parallel fashion. Specifically, the magnitude and frequency of the imposed driving magnetic fields are used as selection methods among the Mag-μBots. Various methods for accomplishing motion discrimination are discussed, modeled, and tested. It is found that while fully decoupled control is not possible with this method, parallel actuation of sub-groups of Mag-μBots is possible and controllable.

1 Introduction

A challenge in the field of micro-robotics is the control of multiple untethered agents. This is particularly difficult with micro-robotic systems because all agents often receive the same driving signal, as in electrostatic (Donald et al. (2008); Sakar et al. (2010)) and electromagnetic (Frutiger et al. (2009); Ghosh and Fischer (2009); Pawashe et al. (2009b); Yamazaki et al. (2004); Zhang et al. (2009)) systems. Methods to address individual micro-robots must be developed for the control of multiple micro-robots to be successful. In our previous works (Floyd et al. (2009a); Pawashe et al. (2009a)), we have shown that multiple identical magnetic micro-robots can be addressed in either an individual serial or coupled parallel fashion. This comes at the cost of requiring a specialized surface that generates spatially local electric fields, and maintaining a minimum distance between the micro-robots.

Using electrostatic actuation, (Donald et al. (2008)) have controlled up to 4 MEMS micro-robots in parallel, by designing individuals to be mechanically unique so that they respond differently to global driving fields generated by the structured substrate. They have established a set of control signals that causes individuals to either turn in circles or translate. Using five such control signals, they can command between 0 and 4 of their robots to turn. In this way, a library of motion primitives has been created, and by using sophisticated algorithms, paths are designed to move from initial to final configurations of the 4 micro-robots. Because of the need for 'stationary' individuals to turn repeatedly in circles, this methodology imposes limits on the amount of free space each individual micro-robot requires.

Using resonant magnetic micro-robots, (Frutiger et al. (2009); Kratochvil et al. (2009)) have demonstrated that decoupled motion is possible with two mechanically unique micro-robots possessing different resonant frequencies; the frequency of the driving magnetic field is varied to select each micro-robot. Similar to (Donald et al. (2008)), these individual micro-robots must be physically unique so that their responses to the global driving magnetic fields differ. Some separation must be maintained between these magnetic micro-robots to keep them from jumping into contact due to magnetic attraction. In addition, by using devices with highly different resonant frequencies, control is often serial, and time multiplexing of the driving signals must be used to achieve the appearance of simultaneous motion control. While individual devices of this type have been reported to operate on unstructured surfaces, such as a clean silicon wafer, all demonstrated multi-robot operation has been done using a structured substrate that generates electrostatic fields. The authors report that this is due to drifting and backwards motion that can occur when not using such a surface. However, in principle, this resonant frequency method could be used to control multiple micro-robots without a specialized surface, once these undesired behaviors have been understood and accounted for.

In this work, we describe methods to control multiple magnetic micro-robots without the need for a specialized substrate. Individual micro-robots themselves can operate on arbitrary surfaces (Pawashe et al. (2009b)); to address multiple agents, we propose designing these micro-robots to respond uniquely to the global driving magnetic fields, similar to (Donald et al. (2008); Frutiger et al. (2009)).

Without the need for a specialized surface, the proposed approach allows multiple micro-robots to operate in a wider range of environments. For example, specialized electrostatic surfaces as in (Donald et al. (2008); Floyd et al. (2009a); Frutiger et al. (2009); Pawashe et al. (2009a)) cannot be operated in ionic

*S. Floyd was with the Department of Mechanical Engineering, Carnegie Mellon University, Pittsburgh, PA 15213, USA. He is now with Arete Associates, Arlington VA 22202, USA.

†E. Diller, and C. Pawashe are with the Department of Mechanical Engineering, Carnegie Mellon University, Pittsburgh, PA 15213, USA

‡M. Sitti is with the Department of Mechanical Engineering and Robotics Institute, Carnegie Mellon University, Pittsburgh, PA 15213, USA; correspondance can be made to: msitti@andrew.cmu.edu

environments, such as in fluids that support biological organisms, due to electrical breakdown. Bypassing this limitation will allow the proposed approach to be used in applications such as bio-manipulation. Further, this approach will also allow these magnetic micro-robots to operate in groups while taking full advantage of their robust nature, working cooperatively on surfaces with large features and roughness, as demonstrated with an individual on a dime in Pawashe et al. (2009b).

2 Tools and System

The magnetic micro-robots (Mag-μBots) described in this work are actuated by six independent electromagnetic coils, aligned to the faces of a cube approximately 11 cm on a side, with horizontal and vertical coils each capable of producing maximum field strengths at the position of the Mag-μBot (see Fig. 1) of 2.8 mT and 2.2 mT, respectively. Imaging of the Mag-μBots and workspace is accomplished by a camera (Sony XC-75 or Pixelink PL-B771F) connected to a variable magnification microscope lens, providing up to a 9.0 mm $\times$ 9.0 mm field of view. Control of the electromagnetic coils is performed by a PC with data acquisition system at a control bandwidth of 1 kHz, and the coils are powered by custom-made electronic amplifiers. Calibration of the fields is performed using a hall-effect sensor placed at the position of the locomotion surface.

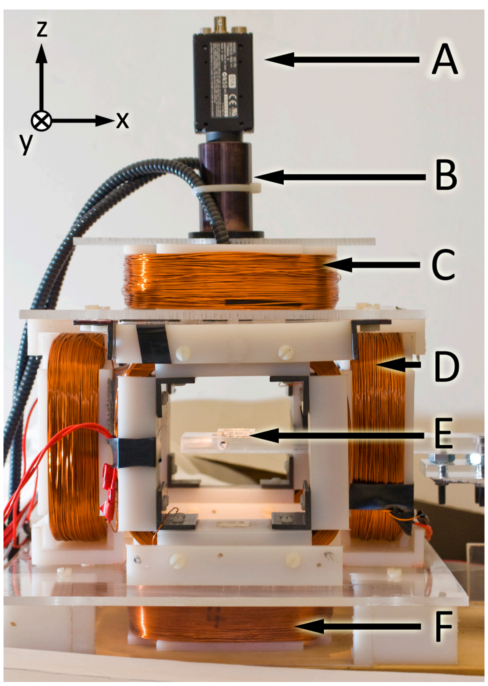

Figure 1: Photograph of the electromagnetic coil setup, where A is the camera for visual feedback, B is the microscope lens, C is the top coil, D is one of four upright coils that orients the Mag-μBot within the plane on the surface, E is the surface on which the Mag-μBot locomotes, and F is the bottom coil. The top and bottom coils are clamping coils, which provide a clamping force and a torque that pushes and orients the Mag-μBot towards the surface, respectively.

Actuation of each Mag-μBot is accomplished by using two or more electromagnetic coils. One or more horizontal coils are first enabled (coil D in Fig. 1), causing the Mag-μBot to orient in the direction of the net magnetic field. The magnetic force exerted by the coils on the Mag-μBot is insufficient to translate it due to high friction and adhesion with the surface. Therefore, vertical clamping coils (coils C and F in Fig. 1) are pulsed using a sawtooth waveform, which causes a rocking motion in the Mag-μBot. During the sharp change in the sawtooth waveform, the Mag-μBot momentarily slips on the surface due to its high angular acceleration, resulting in controllable stick-slip motion across the surface. Typically, a rectilinear Mag-μBot's velocity can exceed 60 body lengths per second in air and 40 body lengths per second in water. The Mag-μBot is also capable of operating in fluids of viscosities of up to 50 cSt, and can operate on a variety of smooth and rough magnetically inactive surfaces, provided that the adhesion between the Mag-μBot and surface is low. Additionally, the pulsed nature of the motion allows the Mag-μBot to be moved in steps as small as 5 μm with an appropriate driving waveform.

Further details of this system are explained in (Floyd et al. (2009b); Pawashe et al. (2009b)), where modeling of the stick-slip dynamics is performed, experimental analyses of robot motion are presented, and micro-particle manipulation is investigated.

Individual Mag-μBots are fabricated to be either magnetically hard, retaining their internal magnetization in the absence of a magnetic field, or magnetically soft, having an internal magnetization that is dependent upon the applied field. Both types of Mag-μBots are fabricated in a batch process using molding techniques in a manner similar to (Imbaby et al. (2008)). Hard Mag-μBots are composed of a mixture of neodymium-iron-boron (NdFeB) particles (Magnequench MQP-15-7, refined in a ball mill to under 2 μm in size) suspended in a polyurethane (TC-892, BJB enterprises) matrix. Soft Mag-μBots use milled iron particles in place of NdFeB. The fabrication process used is shown in Fig. 2.

3 Modeling

On an arbitrary surface, a Mag-μBot will potentially experience electromagnetic, gravitational, adhesive, frictional, and fluid forces from the environment. The effects of these forces are explained in detail in (Pawashe et al. (2009b)). Friction forces are dependent on the materials comprising the Mag-μBot and the surface while adhesive forces are dependent on the composition of the Mag-μBot, the surface and the surrounding fluid.

This section provides derivations of the relevant forces and torques, and examines the conditions necessary for successful selective actuation of a unique Mag-μBot. A schematic of a typical Mag-μBot is shown in Fig. 3.

3.1 Magnetic Torque

The magnetic torque ($\vec{T}_m$) is a function of the volume of the Mag-μBot (V_m), its magnetization ($\vec{M}$), and the applied field ($\vec{B}$):

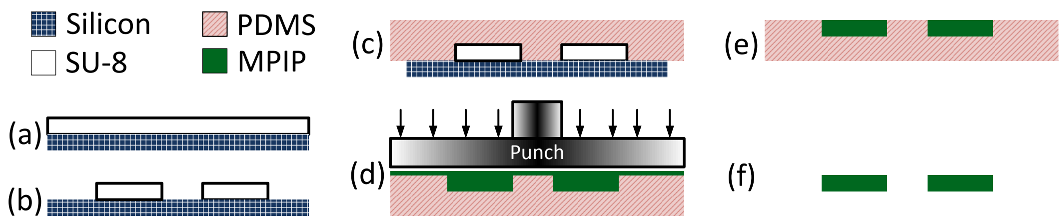

Figure 2: The fabrication steps used to batch manufacture polymer Mag-μBots. (a) SU-8 is spin coated onto a silicon wafer to the desired thickness of the final micro-robot, and (b) is patterned and hardened to create the positive mold. (c) Polydimethylsiloxane (PDMS, Dow Corning HS II RTV) mold making material is poured onto the positive mold and allowed to cure. (d) The PDMS is removed from the positive mold, creating the negative mold that is then flipped, and a mixture of magnetic-powder-impregnated polyurethane (MPIP) is prepared by mixing 4 parts NdFeB powder to 1 part polyurethane (by mass), degassed in a vacuum, and then poured onto the PDMS mold. A large permanent magnet (not shown) is placed under the PDMS mold to ensure the NdFeB powder is densely packed in the mold. After a second degassing, a polypropylene flat punch is pressed and held against the mold, which pushes excess NdFeB-polyurethane out, leaving a thin backing layer. Next, the large magnet is moved to the side of the mold so that the NdFeB particles will orient along the lengths of the Mag-μBots, facilitating a higher net magnetization in the length-wise direction, as magnetic domains will be more favorably oriented. (e) After the polyurethane hardens and the punch is removed, excess polyurethane is peeled off manually using tweezers. (f) Finished polymer Mag-μBots are manually removed from the mold using tweezers, and are magnetized in a vibrating sample magnetometer (VSM, Model DMS 1660) to the desired magnetization.

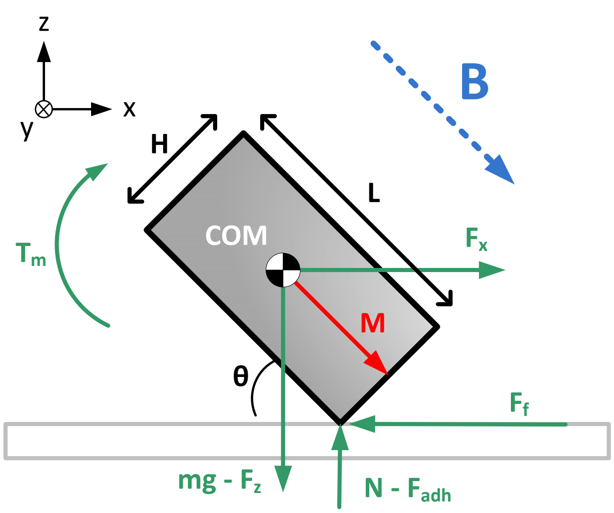

Figure 3: Schematic of a rectilinear Mag-μBot with relevant forces, coordinate system, and center of mass (COM). The magnetic field, B, exerts a torque T_m onto the Mag-μBot that acts to align its magnetization, M, with the field. Forces due to magnetic field gradients exert horizontal and vertical forces on the Mag-μBot, F_x and F_z, respectively. Forces at the contact point with the surface include the normal force, N, adhesion forces, F_{adh}, and the friction force, F_f.

$$\vec{T}_m = V_m \vec{M} \times \vec{B} \tag{1}$$

While magnetic forces do play a part in the motion of the Mag-μBots (Pawashe et al. (2009b)), their effect is considered negligible when compared to magnetic torques. For example, for a Mag-μBot with dimensions $250 \times 130 \times 100$ μm^3 and magnetization of $M = 200$ kA/m, the magnetic force ($F_m = V_m M \nabla B$) an electromagnet in this system can apply, with a gradient of $\nabla B = 55$ mT/m, is approximately $F_m = 36$ nN. By comparison, using (1), a magnetic torque of $T_m = 1.82 \times 10^{-9}$ N $\cdot$ m can be applied with a field of $B = 2.8$ mT orthogonal to the direction of the Mag-μBot's magnetization. This torque, when treated as a pair of forces acting in opposite directions on the ends of the Mag-μBot, acts as opposing forces each approximately 7.3 μN. Thus, the effects of magnetic torques largely dominate Mag-μBot behavior at this size scale. For this reason, the magnetic forces F_x and F_z are assumed to be negligible in these analyses.

3.2 Gravitational Rest Torque

To achieve stick-slip motion, the magnetic torque must overcome the gravitational rest torque to lift the Mag-μBot onto an edge. For a Mag-μBot with side length L along the direction of magnetization, in a gravitational field g, the gravitational rest torque, T_g, is roughly:

$$T_g = \rho_{eff} V_m g \frac{L}{2} \tag{2}$$

where $\rho_{eff} = \rho - \rho_{fluid}$ is the effective density of a Mag-μBot when operating within a fluid. ρ is the actual density of the Mag-μBot, and ρ_{fluid} is the density of the fluid.

3.3 Other Forces and Torques

Depending upon the operational environment and the system used, other forces, including surface adhesion, electrostatic attraction and viscous damping, may also act on the Mag-μBot. These forces are dependent upon the surface energy and dielectric properties of the materials used for both the surface and the Mag-μBot as well as the medium in which the micro-robot operates (Floyd et al. (2009a,b); Pawashe et al. (2009a)). All experiments in this work were performed using polymer-based Mag-μBots on a glass surface while operating in water. For these materials, van der Waals based surface adhesion and electrostatic adhesion can be neglected. Based on the surface energies of polymer, glass, and water, the van der Waals surface adhesion will be repulsive, implying zero adhesion force (Floyd et al. (2009b)). Because water is used, which is slightly conductive, the large electric fields necessary for the generation of electrostatic forces do not occur, negating the effects of any electrostatic forces (Arai et al. (1995)). These forces will be disregarded, but it should be noted that in any situation where they must be considered, these forces will increase the rest torque when $\theta \approx 0$, making it more difficult for a Mag-μBot to rise up onto its edge.

3.4 Natural Frequency

When the Mag-μBot is at an angle to the surface, as shown in Fig. 3, it reacts to changes in the angle of the magnetic field in a manner similar to a rotational spring-mass system. Linearizing (1) provides an analog of a rotational spring, and leads to a rotational natural frequency (ω_n) of:

$$\omega_n = \sqrt{\frac{\frac{\partial T_m}{\partial \theta}}{J}} = \sqrt{\frac{V_m M B}{J}} = \sqrt{\frac{12 M B}{\rho (L^2 + H^2)}} \qquad (3)$$

where $J = \frac{1}{12}\rho V_m (L^2 + H^2)$ is the rotational inertia of a rectilinear Mag-μBot about the y-axis.

Because of the nature of the periodic stick-slip locomotion style, each oscillation requires that a portion of the rotational motion occurs at a higher angular velocity than the rest: the slip phase. Hence, for a given base excitation frequency, several harmonics are required to successfully create the stick-slip rocking motion. As the excitation frequency increases, higher order harmonics will become suppressed and the stick-slip motion will be impeded, reducing micro-robot velocity.

For a Mag-μBot with dimensions $600 \times 300 \times 140$ μm^3 and with $M = 80$ kA/m (slightly larger than the highest value for the hard polymer-based magnets used in this work), at $B = 3.6$ mT, using (3), the rotational natural frequency will be approximately 186 Hz. This value is an effective upper limit for the natural frequencies of the Mag-μBots used in this work, and several have much lower natural frequencies. This frequency is not significantly higher than the magnetic field oscillation frequencies of 1-100 Hz used for actuation of the Mag-μBots. Hence, many of the results in this work show marked roll-off at higher frequencies, especially for those Mag-μBots with lower magnetization values or higher rotational inertias.

4 Selection Methods

The goal of this work is to establish the means by which several Mag-μBots can be controlled simultaneously without the use of any specialized substrate. Because the driving magnetic field will be the same for any Mag-μBots in the workspace, each micro-robot must be inherently unique in order to respond differently. By choosing appropriate values for magnitude, direction, and frequency of the magnetic field, all, none, or some of the Mag-μBots in the workspace can be selected and translated. This concept is shown schematically in Fig. 4.

There are several means by which Mag-μBots can be made to respond differently to the global magnetic fields. First, there are geometric differences between Mag-μBots, controlled by adjusting their aspect ratio and volume. Another method involves changing intrinsic properties of the Mag-μBots, such as magnetization, to achieve different velocity profiles.

Both geometric and magnetization differences are examined in this work for magnetically hard and soft Mag-μBots. These differences are used to determine magnetic states wherein only certain Mag-μBots move. Manufacturing non-uniformities will lead to variations from 'ideal' parameters for any micron-scale systems. As such, the differences between the various Mag-μBot species must be significant enough that they are not overwhelmed by such defects. It is not the goal of the authors to hone in on the exact number of unique Mag-μBots that can be created using the methods described in this work, but to establish the validity of using these methods as a new strategy for parallel control of magnetic micro-robots.

We propose and discuss three selection methods to address multiple Mag-μBots: (1) *Selection via Internal Magnetization*, (2) *Selection via Shape Demagnetization Factor*, and (3) *Selection via Rotational Inertia.*

4.1 Method 1: Selection via Internal Magnetization

One method to discriminate between various Mag-μBots is to use individuals that are geometrically identical within the limits of fabrication, but possess different values of magnetization. Assuming all individuals begin lying flat on the surface, with an applied B, only those individuals with magnetization values in excess of M_{min} will experience magnetic torques large enough to overcome T_g, shown schematically in Fig. 5. Using (1) and (2), M_{min} is derived:

$$M_{min} = \frac{\rho_{eff} g L}{2 B \sin\phi} \qquad (4)$$

where ϕ is the maximum desired angle between the applied field and the robot's orientation. If it is assumed $\phi < 10°$, $\rho_{eff} = 4400$ kg/m^3, $L = 600$ μm and $B = 3.6$ mT, then $M_{min} \approx 20$ kA/m. Hence, for smaller values of B, only individuals with larger internal magnetizations will locomote. As the magnetic field is increased, individuals with progressively lower values of magnetization will be able to overcome T_g and begin to move.

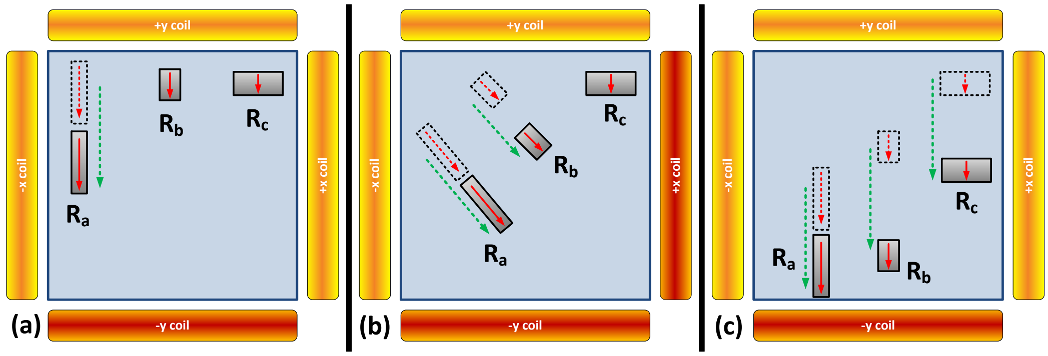

Figure 4: Schematic of three Mag-μBots that respond differently to the imposed magnetic waveform. (a) The first waveform only causes Mag-μBot A to translate. (b) A second waveform causes both A and B to translate together at different velocities. (c) The third waveform causes all 3 Mag-μBots to translate together at different velocities.

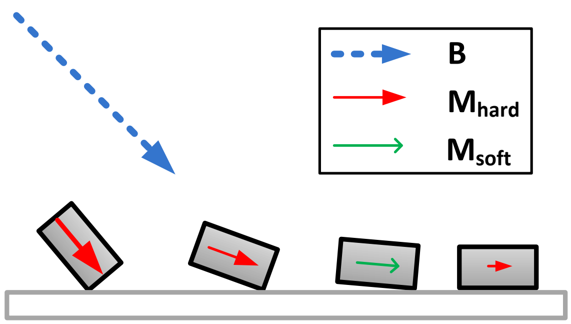

Figure 5: Schematic of three magnetically hard Mag-μBots (M_{hard}) and one magnetically soft Mag-μBot (M_{soft}) with similar geometry whose internal magnetization causes them each to behave differently within applied magnetic fields. Magnetization strength is proportional to arrow length, and the magnetic field direction is shown (blue arrow). The rightmost Mag-μBot is weakly magnetized, and cannot overcome the gravitational rest torque T_g with the given applied field B.

4.2 Method 2: Selection via Shape Demagnetization Factor

Unlike hard magnetic materials, the internal magnetization of magnetically soft Mag-μBots cannot be set at a constant value regardless of shape or applied field. Nor can the internal magnetization of two geometrically identical soft Mag-μBots be different when they are in the same field. For soft magnetic materials, the internal magnetization (M_{soft}) is a function of the material's magnetic susceptibility (χ), the Mag-μBot geometry, and the applied magnetic field B (O'Handley (2000)):

$$M_{soft} = \frac{\chi}{1 + N_d \chi} \left(\frac{B}{\mu_0} \right) \tag{5}$$

where N_d is the shape demagnetization factor in the direction of the applied field. For the system of units used in this work, this factor is always less than 1, and is inversely proportional to the aspect ratio of an object in a given direction (O'Handley (2000)). For materials with high susceptibility ($\chi \gg 1$) and aspect ratios low enough such that $\chi N_d \gg 1$, (5) reduces to (Abbott et al. (2007)):

$$M_{soft} \approx \frac{1}{N_d} \left(\frac{B}{\mu_0} \right) \tag{6}$$

Therefore, by changing the geometry of soft magnetic Mag-μBots made with a high magnetic susceptibility material, the internal magnetization, and hence the applied magnetic torque, varies with N_d^{-1}. Translation can only occur when the gravitational rest torque is overcome, which requires a minimum B. This is shown schematically in Fig. 6.

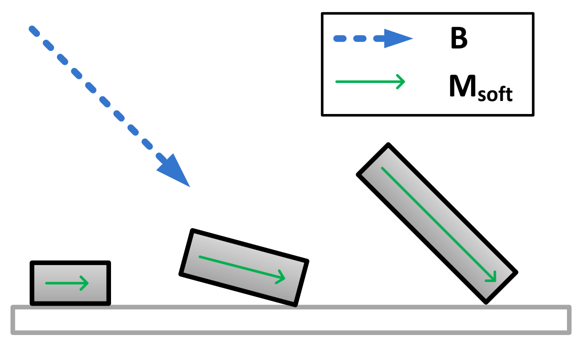

Figure 6: Schematic of three Mag-μBots made of soft magnetic material whose demagnetization factors cause them to behave differently within applied magnetic fields. Magnetization strength is proportional to arrow length, and the magnetic field direction is shown (blue arrow). The leftmost Mag-μBot has the largest demagnetization factor, and cannot overcome the gravatational rest torque with the given B.

We consider two methods for designing unique Mag-μBots using the shape demagnetization factor approach. In the Constant Cross Section Method (CCSM), the cross section of the Mag-μBots is kept constant while the total length is different for each, shown schematically in Fig. 6. In the Constant Length Method (CLM), the total length of the Mag-μBots are kept constant while the cross section is varied. Both of these methods would provide a set of Mag-μBots with different aspect ratios, and thus different demagnetization factors, but only the CLM is effective within a practical range of aspect ratios.

To understand why the CLM is more effective than the CCSM, we examine how the magnetic and gravitational torques scale with the changing aspect ratio. For this analysis, we assume the Mag-μBots have square cross sections, uniform magnetization, and a demagnetization factor similar to that of a prolate ellipsoid of the same aspect ratio, (for which the relationship between aspect ratio and demagnetization factor exists in a closed form). For a prolate ellipsoid magnetized along its major axis, the demagnetization factor becomes (O'Handley (2000)):

$$N_d = \frac{1}{a^2-1}\left\{\frac{a}{\sqrt{a^2-1}}\ln\left[a+\sqrt{a^2-1}\right]-1\right\} \quad (7)$$

$$N_d \approx a^{-2} \quad (8)$$

where a is the aspect ratio of the Mag-μBot's length to its width W and height H. Using these assumptions along with (2), the gravitational rest torques for the CCSM and CLM ($T_{g,CCSM}$ and $T_{g,CLM}$, respectively) scale as follows:

$$T_{g,CCSM} = \frac{1}{2}\rho_{eff}gW^2(aW)^2 \propto a^2 \quad (9)$$

$$T_{g,CLM} = \frac{1}{2}\rho_{eff}g(L/a)^2L^2 \propto a^{-2} \quad (10)$$

Similarly, using (1) and (6), the magnetic torques due to B for the CCSM and CLM ($T_{m,CCSM}$ and $T_{m,CLM}$, respectively) scale as follows:

$$T_{m,CCSM} = W^2(aW)\frac{B}{\mu_0 a^{-2}}B \propto a^3 \quad (11)$$

$$T_{m,CLM} = (L/a)^2L\frac{B}{\mu_0 a^{-2}}B \propto a^0 \quad (12)$$

Examining these results, it is apparent that the ratio of magnetic to gravitational torque increases much more quickly for the CLM than for the CCSM. Employing the exact prolate ellipsoid demagnetization model from (8) and normalizing to an aspect ratio of one, the ratio of magnetic to gravitational torque for the two methods are shown in Fig. 7.

4.3 Method 3: Selection via Rotational Inertia

A third method to select multiple Mag-μBots that can be applied to hard magnetic materials involves utilizing the vibrational response of Mag-μBots of different sizes. The stick-slip motion used to actuate Mag-μBots is composed of periods of both low and high angular velocities and accelerations. When the angular velocity is low, the Mag-μBot rocks on its point of contact with the surface. When the angular velocity is high, the point of contact will slip while the center of mass will translate towards the maximum of any horizontal magnetic field gradient that is present. By using sawtooth or square-type pulsed magnetic field waveforms, the angular rotation during the slip phase is maximized.

From (1), when the magnitude of the magnetization and the magnetic fields are constant, the total maximum magnetic torque is also constant. Angular acceleration, $\ddot{\theta}$, is dependent upon the total torque on the Mag-μBot and its rotational inertia J:

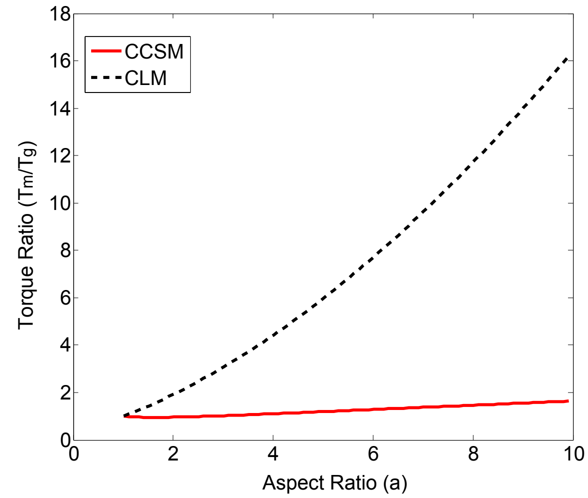

Figure 7: Ratio of magnetic to gravitational torque for different aspect ratios using the Constant Cross Section Method (CCSM) and the Constant Length Method (CLM).

$$\ddot{\theta} = \frac{T_m+T_g}{J} = \frac{T_m+T_g}{\frac{1}{12}\rho_{eff}V_m(L^2+H^2)} \quad (13)$$

The term V_m is present in both the torques and the inertial term, and will cancel out, indicating that the Mag-μBot's volume does not affect its angular acceleration. However, $J \propto L^2$, while $T_g \propto L$, and $T_m \propto L^0$. This implies $\ddot{\theta} \propto L^{-1}$, which indicates that as the characteristic length of the Mag-μBot increases, it experiences enhanced roll-off behavior; this is shown schematically in Fig. 8.

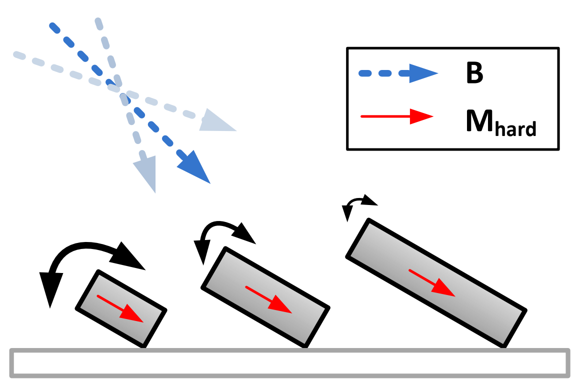

Figure 8: Schematic of three Mag-μBots of similar magnetizations whose size causes them to behave differently within applied magnetic fields. Longer Mag-μBots have higher rotational inertia and hence lower angular acceleration and smaller total angular swing. Magnetization strength is proportional to arrow length, and the oscillating magnetic field is shown (blue arrows).

While the electrical system will itself experience roll-off due to inductance and resistance in the coils, this effect will be constant across the different micro-robot species used and the experiments performed. Hence, any differences among the frequency response behaviors of the micro-robots can be attributed to the robots' properties, and are not inherent in the system. This also implies that sets of micro-robots with natural frequencies much higher than the roll-off of the electrical system would not exhibit high selectivity using the Selection via Rotational Inertia method.

4.4 Combining Selection Methods

Both the magnetic field strength and the oscillation frequency are integral to the control of the velocity of the Mag-μBots, and both of these parameters are varied in the experiments while recording Mag-μBot velocities. At certain frequencies, varying magnetic field strength can be used as a selection method for different Mag-μBots. Similarly, at certain magnetic field strengths, varying the oscillation frequency can also be used as a selection method. Therefore, incorporating both inertial and magnetization differences among Mag-μBots can allow for more complete discrimination by combining effects, or can allow an increase in the total number of controllable Mag-μBots by expanding the number of ways in which individuals can be made unique. This is more easily achieved in hard magnetic Mag-μBots, where the geometry and the magnetization are not strongly linked, as opposed to soft magnetic Mag-μBots, where these two parameters are intimately coupled.

5 Results and Discussion

For each experiment, at least three trials were performed where the Mag-μBots were translated in one direction (toward the +x coil) by teleoperation for several millimeters, while experimental video of the motion was recorded. In post-processing, the average translational velocity was determined by taking two frames of the video, one near the beginning and one near the end of the Mag-μBot's path. In each frame, the robot's position was determined, and the total travel distance was measured in pixels. Using the travel time and a conversion ratio from the image to actual distance, the velocity was determined. Across a travel distance of about 5 mm, a positioning error of 1-2 pixels (about 26 μm) results in a 0.5% error in measured distance.

For *Method 1: Selection via Internal Magnetization*, three hard magnetic Mag-μBots with similar geometry and different values of internal magnetization were used, with the expectation that the Mag-μBot with the highest magnetization value would operate in the most conditions.

For *Method 2: Selection via Shape Demagnetization Factor*, three soft magnetic Mag-μBots with different aspect ratios were used, with the expectation that the Mag-μBot with the highest aspect ratio would operate in the most conditions.

For *Method 3: Selection via Rotational Inertia*, three hard magnetic Mag-μBots with the same magnetization but different aspect ratios were used, with the expectation that the Mag-μBot with the lowest aspect ratio (and thus the lowest inertia) would operate in the most conditions.

Robot	**L (μm)**	**W (μm)**	**H (μm)**	**Moment (mEMU)**	**M (kA/m)**
R_1	569	338	157	2.04	67.6
R_2	556	343	142	1.05	38.7
R_3	594	330	148	0.46	15.8

Table 1: Properties of Similar Geometry, Dissimilar Magnetization, Hard Heterogeneous Mag-μBots.

All experiments were performed on a glass surface under water. An aqueous environment was chosen to reduce adhesion between the Mag-μBots and the glass surface, resulting in less variations in the velocities at each testing condition. For magnetically hard Mag-μBots containing NdFeB particles, magnetization was imposed in a VSM to appropriate values. For all Mag-μBots, the magnetization direction is along the reported length direction.

For each set of experiments, conditions were changed in two ways: by changing the maximum magnetic field strength of the magnetic fields in the workspace (B_{max}) and by changing the frequency (f) of the sawtooth magnetic field waveform. B_{max} is defined as:

$$B_{max} = \sqrt{B_{x,max}^2 + B_{z,max}^2} \tag{14}$$

where $B_{x,max}$ is the maximum magnetic field in the horizontal, or x-direction, and $B_{z,max}$ is the maximum magnetic field seen in the vertical, or z-direction.

5.1 Method 1: Selection via Internal Magnetization

Figure 9 shows the number of Mag-μBots with similar geometries and dissimilar magnetization values that moved under each set of conditions tested, without regard for the velocity of translation. Geometric and magnetic properties for these three Mag-μBots are listed in Table 1. Higher B_{max} and lower f lead to all three Mag-μBots translating while lower B_{max} and higher f lead to fewer Mag-μBots translating. As anticipated, the Mag-μBot with the highest magnetization (R_1) moved in the most conditions.

In order to choose appropriate conditions for selecting the number of moving Mag-μBots, any three locations can be chosen in the experimental state space from Fig. 9, provided that all three motion states (one Mag-μBot moving, two moving, and three moving) are represented in the selection. A simpler method is to keep one parameter (either B_{max} or f) constant while varying the other. In this case, a vertical or horizontal line must be chosen which intersects points of all three motion states. In the case of Fig 9, two such lines exist: a horizontal line at f = 70 Hz, and a vertical line at a B_{max} = 0.82 mT. The full velocity profiles achieved with these two experimental conditions are shown in Figs. 10 and 11, respectively.

From Fig. 10, higher B_{max} corresponded to a larger number of Mag-μBots moving as well as to higher robot veloci-

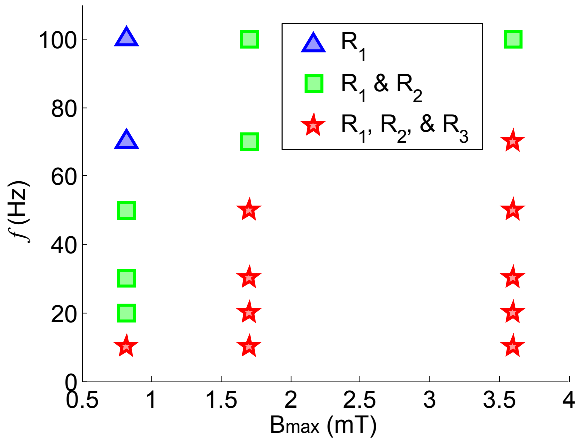

Figure 9: Movement map displaying the number of magnetically hard Mag-μBots with similar geometries and dissimilar magnetization values that translated for each experimental condition. Geometric and magnetic properties of these Mag-μBots are listed in Table 1.

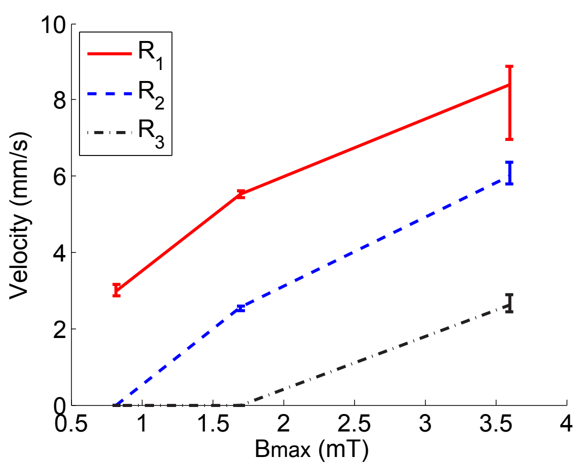

Figure 10: Experimental velocity of three magnetically hard Mag-μBots with similar geometry and dissimilar values of internal magnetization. Oscillation frequency was held constant at 70 Hz. Geometric and magnetic properties of these Mag-μBots are listed in Table 1. Data points are median values and error bars indicate maximum and minimum values.

ties. Also, as anticipated, the Mag-μBot with the highest value of magnetization (R_1) was the most robust, translating under all operational conditions and moving with the highest velocity while the Mag-μBot with the lowest value of magnetization (R_3) moved the slowest and translated under the fewest number of experimental conditions.

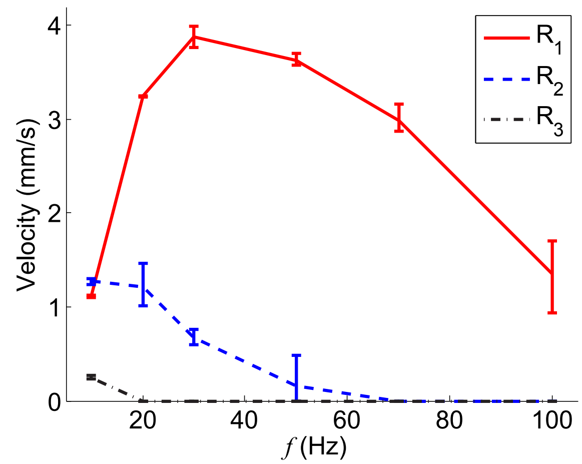

Figure 11: Experimental velocity of three magnetically hard Mag-μBots with similar geometry and dissimilar values of internal magnetization. The maximum field strength was held constant at $B_{max} = 0.82$ mT. Geometric and magnetic properties of these Mag-μBots are listed in Table 1. Data points are median values and error bars indicate maximum and minimum values.

Figure 11 displays the velocity response of the Mag-μBots as a function of f. As estimated in Sec. 3.4, there was a roll-off present in the response of each of the Mag-μBots. As expected, the Mag-μBot with the highest internal magnetization (R_1) translated with the highest velocity over the largest range of f. The Mag-μBot with the lowest magnetization (R_3) only moved at the lowest f.

5.2 Method 2: Selection via Shape Demagnetization Factor

Three geometrically dissimilar Mag-μBots made of soft magnetic material and designed using the CLM from Sec. 4.2 were employed, with the geometric and magnetic properties listed in Table 2. Because magnetization is a function of applied field for soft magnetic materials, the magnetization for each Mag-μBot was determined in a VSM for several applied fields over the range of 0-9 mT, and interpolated to determine the magnetization at the field strengths used in experiments.

At $B_{max} \approx 3.6$ mT (the maximum value used for hard magnets), M is less than 27 kA/m for all of the soft magnetic Mag-μBots. Further, at that field strength, $M_{min} \approx 34$ kA/m, calculated for these Mag-μBots from (4). As a result, these Mag-μBots are immobile for low values of B_{max}. To increase the magnetization in the Mag-μBots, additional electromagnetic coils were used to increase B_{max} to 5.8 mT.

Figure 12 shows the number of Mag-μBots with dissimilar

Robot	L (μm)	W (μm)	H (μm)	M at 5.8 mT (kA/m)
R_4	1036	475	122	26.1
R_5	1059	221	120	34.9
R_6	962	109	117	37.7

Table 2: Properties of Dissimilar Geometry, Dissimilar Magnetization, Soft Heterogeneous Mag-μBots.

shape demagnetization factors that moved under each set of experimental conditions. As with the Selection via Internal Magnetization Value method, higher B_{max} and lower f lead to all three Mag-μBots translating, whereas low B_{max} and high f lead to only one Mag-μBot translating. In this case, it was anticipated that narrower Mag-μBots would be the most effective in translating because they had the lowest demagnetization factor, and hence the highest value of internal magnetization in a given B.

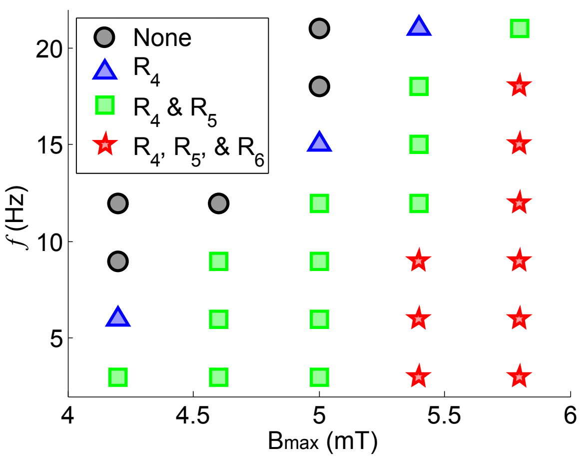

Figure 12: Movement map displaying the number of magnetically soft Mag-μBots with dissimilar geometries which translated for each experimental condition. All data points obscured by the legend represent magnetic field states where no Mag-μBots translated. Geometric and magnetic properties of these Mag-μBots are listed in Table 2.

Horizontal and vertical lines on Fig. 12 that intersect points of all three motion states can be used for control purposes. In this case, two horizontal lines, corresponding to $f = 6$ Hz and $f = 15$ Hz are both plausible, and yield the velocity profiles shown in Figs. 13 and 14, respectively. In addition, a vertical line drawn at $B_{max} = 5.4$ mT is also possible, producing the results shown in Fig. 15.

In Fig. 13, Mag-μBots with higher aspect ratios (and thus smaller N_d) are more robust, responding with higher velocities and operating at lower magnetic fields. Surprisingly, the Mag-μBot with the highest magnetization (R_6) does not always move with the highest velocity. This may be due to the fact that despite the narrowest Mag-μBot (R_6) being half the width of the second narrowest (R_5), the two have very similar values of

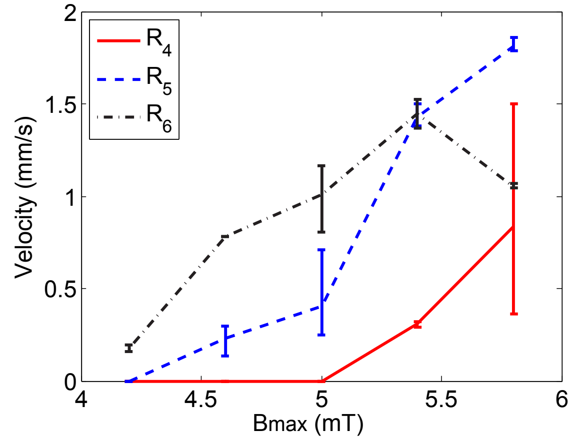

Figure 13: Experimental velocity of the three magnetically soft Mag-μBots with dissimilar geometry and hence dissimilar values of internal magnetization. Oscillation frequency is held constant at 6 Hz. Geometric and magnetic properties of these Mag-μBots are listed in Table 2. Data points are median values and error bars indicate maximum and minimum values.

magnetization.

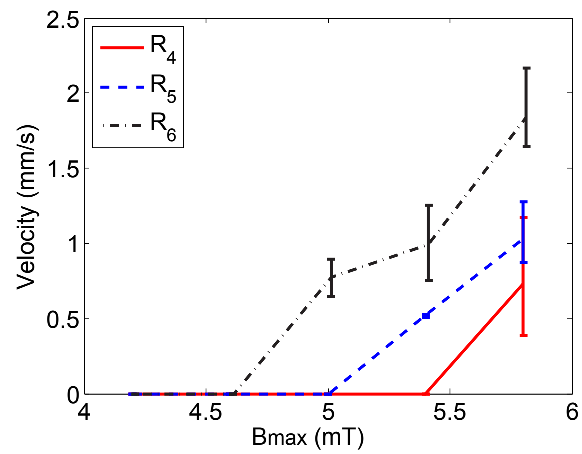

Figure 14: Experimental velocity of the three magnetically soft Mag-μBots with dissimilar geometry, and hence dissimilar values of internal magnetization. Oscillation frequency is held constant at 15 Hz. Geometric and magnetic properties of these Mag-μBots are listed in Table 2. Data points are median values and error bars indicate maximum and minimum values.

Figure 14 shows Mag-μBot responses that agreed with expectations. The Mag-μBot with the highest value of magnetization (R_6) translated with the highest velocity under the largest range of parameter variations, while the Mag-μBot with the lowest value of magnetization (R_4) was the slowest and operated under the fewest operating conditions. Velocities for all three Mag-μBots increased with increasing B_{max}.

Holding B_{max} constant while varying f produced the results shown in Fig. 15. Mag-μBots R_5 and R_6 have very similar values of magnetization, despite the factor of two difference in their aspect ratios. Besides the response at $f = 21$ Hz, this

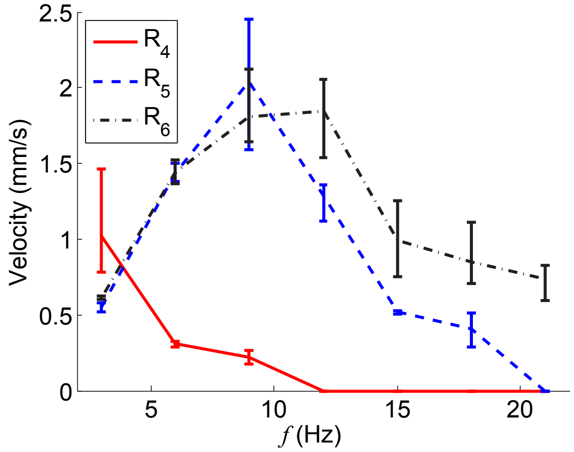

Figure 15: Experimental velocity of the three magnetically soft Mag-μBots with dissimilar geometry, and hence dissimilar values of internal magnetization. The maximum field strength is held constant at 5.4 mT. Geometric and magnetic properties of these Mag-μBots are listed in Table 2. Data points are median values and error bars indicate maximum and minimum values.

led to very similar velocity profiles, making it more difficult to achieve a control scheme for all three soft Mag-μBots. This similarity may be due to all three magnetically soft Mag-μBots having similar heights, potentially mitigating the effects of the different aspect ratios. To more successfully utilize this form of Mag-μBot selection, perhaps square cross sections with different side lengths could be used with Mag-μBots possessing the same length. Unfortunately, manufacturing such Mag-μBots simultaneously with the process shown in Fig. 2 would require them to be fabricated in a vertical orientation, which is difficult for shapes a millimeter in total length.

5.3 Method 3: Selection via Rotational Inertia

Three geometrically dissimilar magnetically hard Mag-μBots were magnetized in a VSM to have similar values of magnetization. In addition to magnetization, the height and width of the Mag-μBots were kept similar, with the values listed in Table 6.

Robot	L (μm)	W (μm)	H (μm)	Moment (mEMU)	M (kA/m)
R_7	328	154	91	0.24	50.6
R_8	502	166	84	0.34	49.0
R_9	840	178	69	0.52	50.2

Table 3: Properties of Dissimilar Geometry, Similar Magnetization, Hard Heterogeneous Mag-μBots.

Figure 16 shows the number of Mag-μBots that moved under each set of experimental conditions. Higher B_{max} and lower f led to all three Mag-μBots locomoting, whereas lower B_{max} and higher f led to only one moving. From Sec. 4.3, the shortest of the three Mag-μBots (R_7) was expected to be the most robust due to its higher roll-off frequency, while the longest (R_9) was expected to move under the fewest experimental conditions due to its lower roll-off frequency. From Fig. 16, there exists only one line which intersects all points of all three motion states, i.e. when $B_{max} = 0.86$ mT. There existed no f at which all three motion states occur while varying B_{max}.

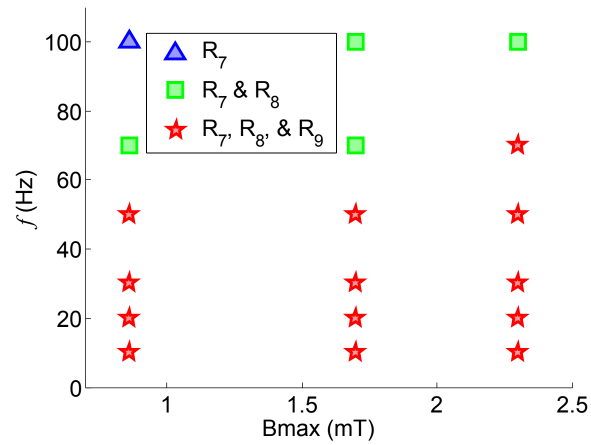

Figure 16: Movement map displaying the number of magnetically hard Mag-μBots with similar magnetization values and dissimilar geometries which translated for each experimental condition. Geometric and magnetic properties of these Mag-μBots are listed in Table 6.

In Fig. 17, $B_{max} = 0.86$ mT while f was varied for the three Mag-μBots. The shortest Mag-μBot's (R_7) velocity began to roll-off at $f = 50$ Hz, the medium length Mag-μBot's (R_8) velocity began to roll-off at $f = 30$ Hz, while the longest Mag-μBot's (R_9) velocity began to roll-off at $f = 20$ Hz. Consistent with Fig. 16, the shortest Mag-μBot (R_7) operated under the most conditions while the longest (R_9) operated under the least number of conditions.

Given the trends in the movement map shown in Fig. 16, it is likely that at a higher B_{max}, all three Mag-μBots would translate at higher frequencies. This could lead to the ability to control all three motion states of these Mag-μBots by varying the B_{max} with a fixed, high f.

5.4 Demonstration

The previously discussed experimental results all corresponded to Mag-μBots being tested one at a time. To demonstrate the feasibility of moving multiple Mag-μBots simultaneously, three Mag-μBots, R_1, R_2, and R_3 were positioned using the methods described in Secs. 4.1 and 5.1. Several frames from a movie of this experiment are displayed in Fig. 18. While independent control of an arbitrary individual was not possible, by establishing the appropriate rules and algorithms, an arbitrary final configuration of Mag-μBots was achieved from an arbitrary initial configuration, similar to the micro-robot control strategy in (Donald et al. (2008)). The net displacements are shown in Fig. 18(f).

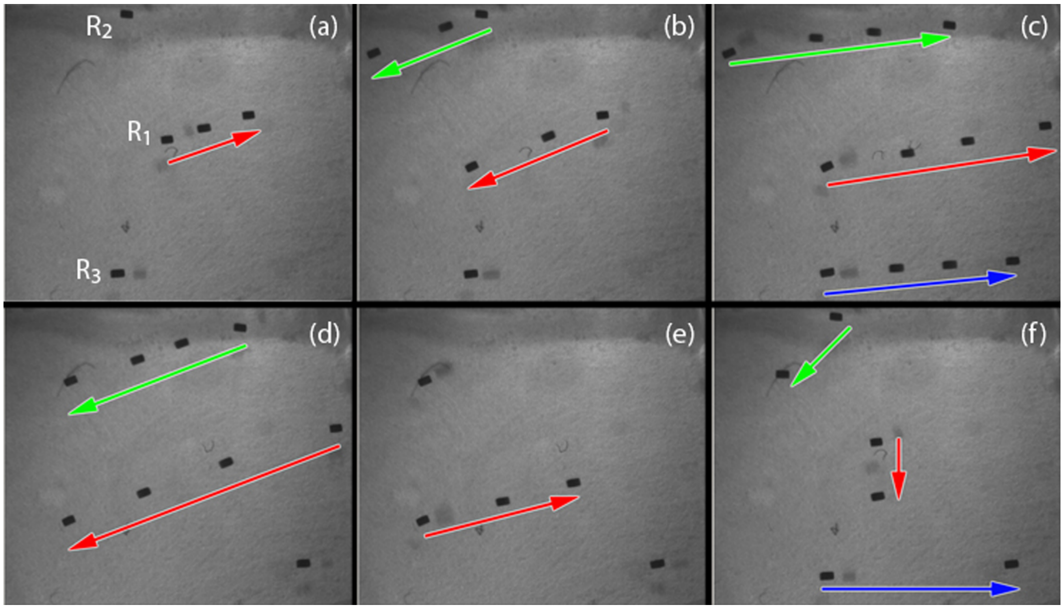

Figure 18: Frames from a movie with three Mag-μBots, R_1, R_2, and R_3 traversing individually and in parallel while operating in water on an unstructured glass surface. (a) A state was chosen from Fig. 9 where only R_1 translated. (b) A different state was chosen that allowed both R_1 and R_2 to translate. (c) All three translated when a third state is chosen. (d) Again, a state was chosen where only R_1 and R_2 translated. (e) A final state was chosen where only R_1 moved. (f) Net motion from initial configuration to a 'desired' configuration near the end of the experiment. Each micro-robot effectively moved in a direction independent of the other two. Geometric and magnetic properties of these Mag-μBots are listed in Table 1. Video available in Extension 1.

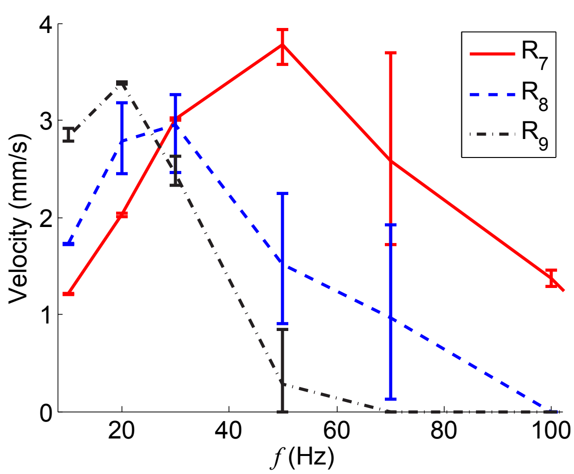

Figure 17: Experimental velocity of the three magnetically hard Mag-μBots with dissimilar geometry and similar values of internal magnetization. The maximum field strength was held constant at 0.86 mT. Geometric and magnetic properties of these Mag-μBots are listed in Table 6. Data points are median values and error bars indicate maximum and minimum values.

6 Conclusions

Three methods for the control of heterogeneous groups of magnetic micro-robots were demonstrated. In each method, three Mag-μBots were controlled in a coupled fashion that allows for independent global positioning of each micro-robot. For each method, the Mag-μBots were fabricated with unique properties so that they responded differently to the actuation magnetic fields. In the first method, three geometrically similar Mag-μBots were fabricated with magnetically hard materials and different levels of internal magnetization. Magnetically soft Mag-μBots were used in the second method, where the geometry was varied to effectively control the internal magnetization. Lastly, a third method utilized geometrically dissimilar Mag-μBots with similar values of magnetization. Models were developed to explain the principle of operation for each of these methods.

For all three methods of heterogeneous micro-robot control, there existed states of magnetic field strength and oscillation frequency that corresponded to 1, 2, or 3 Mag-μBots moving. By switching between these states, it was possible to effectively generate independent motion of the Mag-μBots.

Future works will include incorporating vision, path planning, and appropriate selection and control algorithms to autonomously control heterogeneous sets of Mag-μBots to perform tasks, such as manipulating micro-scale objects. Additionally, by using time multiplexing of multi-robot control, sets of heterogeneous robots can have the appearance of following straight paths to arbitrary final locations.

Acknowledgment

The authors would like to thank Andrew Gamble and the Carnegie Mellon DSSC for use of the VSM, Magnequench for supplying magnetic powders, and the NanoRobotics Laboratory members for their support and suggestions. This work is supported by the National Science Foundation CAREER award program (NSF IIS-0448042), the NSF Graduate Research Fellowship, and the Bertucci Fellowship.

References

J. Abbott, O. Ergeneman, M. Kummer, A. Hirt, and B. Nelson. Modeling magnetic torque and force for controlled manipulation of soft-magnetic bodies. *IEEE Transactions on Robotics*, 23:1247–1252, 2007.

F. Arai, D. Ando, T. Fukuda, Y. Nonoda, and T. Oota. Micro manipulation based on micro physics - strategy based on attractive force reduction and stress measurement. In *IEEE/RSJ International Conference on Intelligent Robots and Systems*, volume 2, pages 236–241, 1995.

B. Donald, C. Levey, and I. Paprotny. Planar microassembly by parallel actuation of mems microrobots. *Journal of Microelectromechanical Systems*, 17:789–808, 2008.

S. Floyd, C. Pawashe, and M. Sitti. Microparticle manipulation using multiple untethered magnetic microrobots on an electrostatic surface. In *Proceedings of the IEEE/RSJ International Conference on Intelligent Robots and Systems*, pages 528–533, St. Louis, Missouri, 2009a.

S. Floyd, C. Pawashe, and M. Sitti. Two-dimensional contact and non-contact micro-manipulation in liquid using an untethered mobile magnetic micro-robot. *IEEE Transactions on Robotics*, 25:1332–1342, 2009b.

D. R. Frutiger, K. Vollmers, B. E. Kratochvil, and B. J. Nelson. Small, fast, and under control: Wireless resonant magnetic micro-agents. *International Journal of Robotics Research*, 29:613–636, 2009.

A. Ghosh and P. Fischer. Controlled propulsion of artificial magnetic nanostructured propellers. *Nano Letters*, 9:2243–2245, 2009.

M. Imbaby, K. Jiang, and I. Chang. Net shape fabrication of stainless-steel micro machine components from metallic powder. *Journal of Micromechanics and Microengineering*, 18, 2008.

B. Kratochvil, D. Frutiger, K. Vollmers, and B. Nelson. Visual servoing and characterization of resonant magnetic actuators for decoupled locomotion of multiple untethered mobile microrobots. In *IEEE International Conference on Robotics and Automation*, pages 1010–1015, Kobe, Japan, 2009.

R. O'Handley. *Modern Magnetic Materials: Principles and Applications*. John Wiley and Sons, Inc., 2000.

C. Pawashe, S. Floyd, and M. Sitti. Multiple magnetic microrobot control using electrostatic anchoring. *Applied Physics Letters*, 94, 2009a.

C. Pawashe, S. Floyd, and M. Sitti. Modeling and experimental characterization of an untethered magnetic micro-robot. *International Journal of Robotics Research*, 28:1077–1094, 2009b.

M. Sakar, E. B. Steager, A. A. Juliusz, M. Kim, V. Kumar, and G. J. Pappas. Biosensing and actuation for microbiorobots. In *IEEE International Conference on Robotics and Automation*, pages 3141–3146, Anchorage, AK, 2010.

A. Yamazaki, M. Sendoh, K. Ishiyama, K. I. Arai, R. Kato, M. Nakano, and H. Fukunaga. Wireless micro swimming machine with magnetic thin film. *Journal of Magnetism and Magnetic Materials*, 272-276:1741–1742, 2004.

L. Zhang, J. Abbott, L. Dong, B. Kratochvil, D. Bell, and B. Nelson. Artificial bacterial flagella: Fabrication and magnetic control. *Applied Physics Letters*, 94, 2009.

Appendix: Index to Multimedia Extensions

The multimedia extensions to this article are at http://www.ijrr.org.
Table of Multimedia Extensions

Extension	Type	Description
1	Video	Three micro-robots traversing individually and in parallel, corresponding to Figure 18.